A hexa-quinoline based C_3-symmetric chemosensor for dual sensing of zinc(II) and PPi in an aqueous medium *via* chelation induced "OFF–ON–OFF" emission

Sanghamitra Sinha[a], **Bijit Chowdhury** [a], **Nayarassery N. Adarsh**[b] **and Pradyut Ghosh***[a]

[a]*Department of Inorganic Chemistry, Indian Association for the Cultivation of Science, 2A & 2B Raja S. C. Mullick Road, Kolkata 700 032, India. E-mail: icpg@iacs.res.in*

[b]*Instituto Catalan de Nanociencia y Nanotecnologia (ICN2), Edifici ICN2, Campus UAB, Cerdanyola del Valles 08193, Spain*

A quinoline-based C_3-symmetric fluorescent probe (**1**), *N*,*N*′,*N*″-((2,4,6-trimethylbenzene-1,3,5-triyl)tris(methylene))tris(1-(quinolin-2-yl)-*N*-(quinolin-2-ylmethyl)methanamine), has been developed which can selectively detect Zn^{2+} without the interference of Cd^{2+} *via* significant enhancement in emission intensity (fluorescence "turn-ON") associated with distinct fluorescence colour changes and very low detection limits (35.60×10^{-9} M in acetonitrile and 29.45×10^{-8} M in 50% aqueous buffer (10 mM HEPES, pH = 7.4) acetonitrile media). Importantly, this sensor is operative with a broad pH window (pH 4–10). The sensing phenomenon has been duly studied through UV-vis, steady-state, and time-resolved fluorescence spectroscopic methods indicating 1 : 3 stoichiometric binding between **1** and Zn^{2+} which is further corroborated by ^{1}H NMR studies. Density functional theoretical (DFT) calculations provide the optimized molecular geometry and properties of the zinc complex, **1**$[Zn(ClO_4)]_3^{3+}$, which is proposed to be formed in acetonitrile. The results are in line with the solution-state experimental findings. The single crystal X-ray study provides the solid state structure of the trinuclear Zn^{2+} complex

showing solubility in an aqueous buffer (10 mM HEPES, pH = 7.4). Finally, the resulting trinuclear Zn^{2+} complex has been utilized as a fluorescence “turn-OFF” sensor for the selective detection of pyrophosphate in a 70% aqueous buffer (10 mM HEPES, pH = 7.4) acetonitrile solvent with a nanomolar detection limit (45.37×10^{-9} M).

Introduction

Zinc is the second most abundant transition metal occurring in the human body and plays diverse roles in several vital biological processes like cellular metabolism, neurotransmission, *etc*.[1–11] In everyday life, zinc is found in various foods, automobiles, sunscreens, cosmetics and surgical tools *etc*. It exists mostly as Zn^{2+} in the body as well as in nature.[12] However, misregulation of Zn^{2+} causes several diseases like Alzheimer's, epilepsy, infantile diarrhea, prostate cancer, *etc*.[1–11,13–17] On the other hand, pyrophosphate (PPi), which is produced during ATP hydrolysis, is a crucial anion for normal cell functioning, *e.g.*, it is involved in DNA polymerase catalyzed DNA replication and real time DNA sequencing.[18–29] So, it is highly desirable to explore efficient methods to detect and monitor Zn^{2+} and PPi in environmental as well as in biological samples. For this purpose, fluorescence sensors have drawn a lot of attention from the chemistry community because of their various advantages like high sensitivity, simplicity, and versatile instrumentation.[1–5,12,20–26]

Here, it has to be mentioned that, due to the almost similar electronic properties of Cd^{2+} and Zn^{2+}, it is indeed difficult to develop a selective chemosensor for Zn^{2+} without the interference of Cd^{2+}.[30–34] Though an ample number of fluorescence sensors for Zn^{2+} have been reported based on di-2-picolylamine (DPA),[9,10,15–17,35–40] quinoline,[1,8,10,15,35,41–46] bipyridyl[1,47] *etc*. and their derivatives, involving photoinduced electron transfer (PET), intermolecular charge transfer (ICT) and chelation induced enhanced fluorescence (CHEF)

mechanisms,[1–3,8,12,21,48] the number of sensors capable of selectively sensing Zn^{2+} in an aqueous buffer through a wide range of pH values is still limited.[4–6,41,49–51] In this context, among different types of fluorescent zinc sensors, quinoline substituted ligands have been paid much attention due to their well-known chelating property towards soft metals as well as suitable spectral behavior.[1,41,42–46] It has also been observed that, in some cases, an increase in the number of quinoline units in the binding arm improves the sensitivity.[44] Thus, to achieve a highly selective and sensitive chemosensor for Zn^{2+} in an aqueous buffer medium, here we introduce a new quinoline-based fluorescence probe. Furthermore, we also demonstrate that the Zn^{2+} complex of the ligand can act as a selective pyrophosphate sensor in a 70% aqueous buffer (10 mM HEPES, pH = 7.4).

Results and discussion

Designing aspect of 1

Being ions of similar sizes (radius of Zn^{2+} is only 21 pm shorter than that of Cd^{2+})[30] it is quite difficult to discriminate Zn^{2+} and Cd^{2+} using some chelating fluorophoric systems. Thus the choice of the platform, chelating unit and the sensing system should be cleverly designed to obtain selectivity for a particular metal analyte over its common interferrants. In this context, C_3-symmetric ligands,[52a–c] which have the potential to develop a suitable receptor to meet the required coordination environment of metal ions, are of real importance. Furthermore, there are plenty of reports in the literature showing Zn(II) sensing towards mononuclear or binuclear di-picolyl amine or quinolone-based ligands.[1,52d] Our group also reported a selective Zn(II) sensor where two quinoline units were used to chelate with Zn^{2+}.[45] Keeping this in mind, an easily synthesizable ligand, **1** (Chart 1), has been designed where six quinoline moieties have been

incorporated into an arene platform to enhance the aqueous solubility of the sensor molecule as well as to create a sterically crowded environment, expecting that it could provide better fitting toward Zn^{2+} than the closely related analyte Cd^{2+}. Furthermore, the sensor with six flexible side arms is expected to have a non-luminescent nature due to better non-radiative decay. However, the coordination of multiple metal centres with the multiple side arms is expected to rigidify the overall system effectively, which might result in a drastic enhancement in the fluorescence output. On the other hand, the sensor with multiple Zn^{2+} sites would be a potential candidate for screening phosphates including its higher analogues.[52–69]

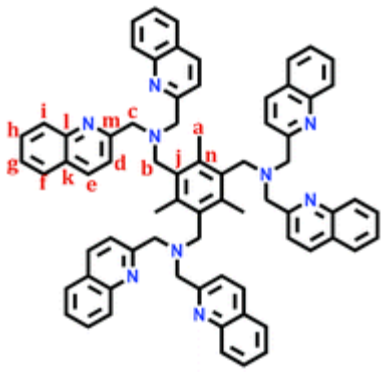

Chart 1 Chemical structure of the ligand **1**.

Synthesis and characterization

The sensor **1** is synthesized by refluxing 1,3,5-tris(aminomethyl)-2,4,6-trimethylbenzene and 2-(chloromethyl)quinoline hydrochloride in dry acetonitrile in the presence of K_2CO_3 and a catalytic amount of KI for 12 h (Scheme 1). **1** is fully characterized by 1D (^1H, DEPT-135, and ^{13}C) and 2D (^1H–^1H COSY, ^1H-DEPT-135 HSQC and ^1H–^{13}C HMBC) NMR spectroscopy, electrospray ionization mass spectrometry (Fig. S1–S7, ESI†) and elemental analysis techniques. In the NMR spectrum of **1**, all the protons and carbons resonate in their expected frequency ranges in $CDCl_3$ (in 300 MHz) at room

temperature, which are properly assigned with the help of corresponding $^{1}H–^{1}H$ COSY, ^{1}H-DEPT-135 HSQC and $^{1}H–^{13}C$ HMBC experiments. The peak for the molecular ion ($[C_{72}H_{63}N_9][H^+]$) is observed in the ESI-MS of **1** at 1054.51 (calculated 1054.33). The single crystal X-ray structural analysis shows that the ligand crystallizes in the monoclinic $P2_1/c$ space group where three quinoline arms arrange themselves in the opposite direction with respect to the other three. The details of the structure are given in Fig. S8 and Table S1, ESI.†

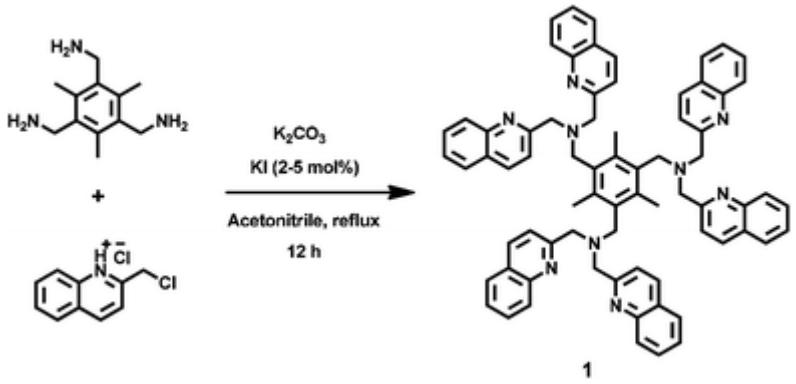

Scheme 1 Synthetic procedure for the ligand **1**.

Zn^{2+} sensing studies in acetonitrile

A detailed study about the photophysical properties of **1** is conducted using absorbance (UV-visible), photoluminescence (PL), and time-resolved spectroscopic methods. A prominent signature of the quinoline unit is observed in the absorption spectrum of **1** which contains absorption bands at ~210 (ε = 111 420 M^{-1} cm^{-1}), ~240 (ε = 116 552 M^{-1} cm^{-1}), ~303 (ε = 26 854 M^{-1} cm^{-1}) and ~315 (ε = 23 287 M^{-1} cm^{-1}) nm in acetonitrile at 25 °C (Fig. S9a, ESI†). Among these, the bands at 210 and 240 nm might originate from the intra-ligand (IL) π–π* electronic transitions while the bands at 303 and 315 nm

may arise from the n–π* transitions *i.e.* the electronic transitions from nonbonding orbitals on the nitrogen atoms (amine and quinoline) to ligand π* orbitals.[70,71] Initially the ligand is very weakly emissive; illumination at the 315 nm wavelength results in a broad centered weak emission band at 430 nm resulting in a light green photoluminescence (Fig. S9a, ESI†). The weak emission may be the result of inner quenching of fluorescence due to the contribution of non-bonding electrons. In quinoline-based molecules like **1**, the n–π* singlet and π–π* singlet transitions are energetically not very far. Hence, though the π–π* singlet transition occurred directly upon excitation, it might have a large propensity to transfer to the n–π* singlet. And once the π–π* singlet → n–π* singlet transfer takes place, it is consequently followed by an inter-system crossing (ISC) from n–π* singlet → n–π* triplet with a considerable ease.[70,71] Thus, the n–π* triplet state makes these molecules very weakly luminescent. To check whether the ligand is selective toward any metal ion, metal binding properties of **1** are explored in acetonitrile. The changes in its spectral behavior in the presence of different metal ions are studied using the acetonitrile solutions of their corresponding perchlorate salts. The addition of 10 equiv. of various metal ions except Zn^{2+} to 6.5×10^{-5} M solution of **1** in acetonitrile does not result in any remarkable changes in the absorption spectrum, whereas, in the presence of Zn^{2+}, an increase in the absorbance values at 303 and 315 nm is observed with the formation of a clear isosbestic point at 290 nm (Fig. S9b, ESI†). A huge change is noticed in the emission profile of the ligand (8.5×10^{-6} M in acetonitrile) upon the addition of 10 equiv. of Zn^{2+} (Fig. 1). The very weak broad centered emission band of the ligand is changed to a sharp peak with 63-fold enhancement in emission intensity. The emission maximum is blue-shifted to 400 nm associated with a fluorescence color change from light green to blue (Fig. 1). However, other metal ions (10 equiv.) do not result in any significant change in the emission spectrum. The increase

in fluorescence intensity in the presence of zinc may be the outcome of the reduced flexibility of the six quinoline arms upon chelation with Zn^{2+} which tends to increase the fluorescence quantum efficiency. Coordination with a metal, on the other hand, stabilizes the non-bonding electrons over nitrogens and as a result the level of the n–π* singlet state might have increased remarkably.[70] This in turn could affect the π–π* singlet → n–π* singlet transition (which occurs easily in the free ligand making the molecule very weakly emissive) to occur and thus the molecule could emit more easily from the π–π* singlet state (*i.e.* highly fluorescent). Besides changing the absorption and emission spectral behavior, the addition of Zn^{2+} also brings about an enhancement in the quantum yield value of **1**. In the case of a free ligand, the value is calculated as 0.0041 considering anthracene as the standard,[71] while it increases to 0.25 upon the addition of Zn^{2+} (Fig. S10, ESI†). The initial very small quantum yield value could easily be correlated with the flexible structure of the ligand which allows the non-radiative decay through rotational and vibrational pathways and hence lowers the emission quantum yield. Coordination with Zn^{2+}*via* quinoline side arms, as mentioned previously, decreases this probability and thus might be responsible for a higher quantum yield in the adduct.

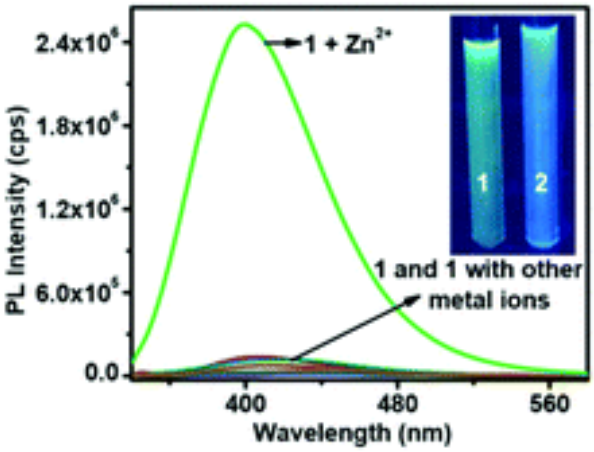

Fig. 1 Emission spectral changes of **1** (8.5×10^{-6} M) in the presence of various metal ions (10 equiv.) as their perchlorate salts, in acetonitrile at room temperature (Inset: Fluorescence colors of (1) **1** and (2) its Zn^{2+} complex in acetonitrile).

To understand the Zn^{2+} binding properties of **1** better, absorption and emission titration experiments are carried out. Incremental addition of Zn^{2+} in 6.5 × 10^{-5} M solution of **1** in acetonitrile promotes an increase in the absorbance at 303 and 315 nm with the formation of a clear isosbestic point at 290 nm (Fig. 2a). In PL titration, the intensity of the emission band gradually increased in the presence of an increasing amount of Zn^{2+}, whereas the broad emission band at 430 nm blue-shifts to give a sharp peak at 400 nm (Fig. 2b). In both the cases (UV-vis and PL titration), the spectral changes are ceased after the addition of 3 equiv. of Zn^{2+} indicating 1 : 3 stoichiometric binding between **1** and Zn^{2+}. This binding stoichiometry is further confirmed by Job plot analysis which shows an inflection point at 0.33 (Fig. S11a, ESI†). The association constant for Zn^{2+} binding by **1** is calculated as K_{Zn1} = 1.23 × 10^5, K_{Zn2} = 9.19 × 10^4, and K_{Zn3} = 6.46 × 10^4 M^{-1} according to the procedure reported in the literature (Fig. S11b, ESI†), whereas the lower limit of the detection of Zn^{2+} by **1** is found to be 35.60 × 10^{-9} M (Fig. 3a) using the calibration curve of change in emission intensity ($I - I_0$) *versus* the concentration of Zn^{2+}. Thus, the sensitivity of **1** appears to be better than that of many of the reported sensors as enlisted in Table S2, ESI.† To check whether the ligand is selective for Zn^{2+} a selectivity study is carried out. The addition of Zn^{2+} in the presence of an excess amount of other metal ions like Mn^{2+}, Mg^{2+}, Cr^{3+}, Cu^{2+}, Cd^{2+}, Ag^{+}, Hg^{2+}, Al^{3+}, Pb^{2+}, Fe^{2+}, Ni^{2+} and Co^{2+} (10 equiv. each) results in the same emission enhancement as observed in the case of only Zn^{2+} (Fig. 3b). Thus, the high association constant values of Zn^{2+} binding by **1** as well as its low limit of detection for Zn^{2+} makes **1** a selective luminescent sensor for Zn^{2+} even in the presence of a large excess of other competitive metal ions in acetonitrile.

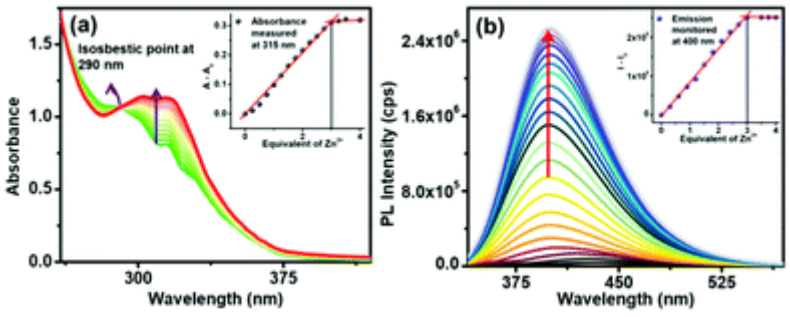

Fig. 2 (a) Absorption (6.5 × 10^{-5} M) and (b) emission (8.5 × 10^{-6} M) titration profiles of **1** with Zn^{2+} in acetonitrile at room temperature. (Inset: Corresponding equivalent plots).

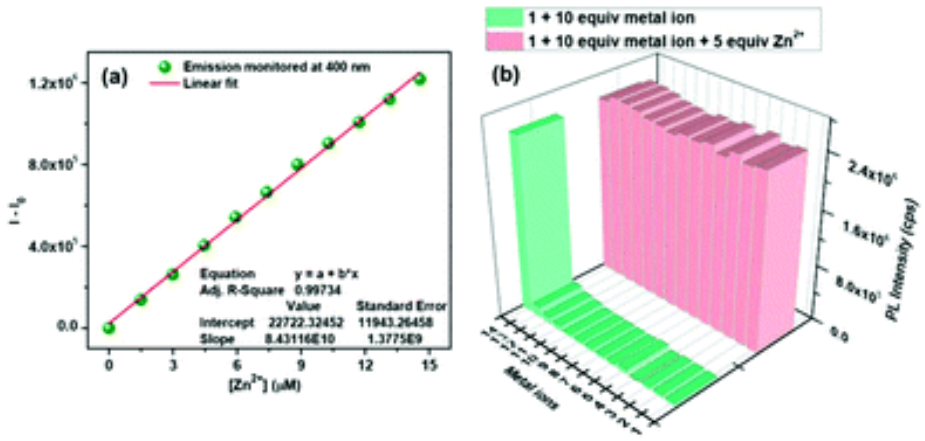

Fig. 3 (a) The calibration curve for Zn^{2+} over the concentration range between 0 and 15 μM derived from the PL titration with **1** (8.5×10^{-6} M) in acetonitrile at room temperature and (b) selectivity graph of **1** with Zn^{2+} in the presence of other metal ions in acetonitrile (λ_{em} = 400 nm). Green bars represent the fluorescence intensities of **1** in the presence of all metal ions (10 equiv.) and the light magenta bars correspond to the same in the presence of all metal ions and Zn^{2+}. Codes used: (1) only **1**, (2) Mn^{2+}, (3) Mg^{2+}, (4) Cu^{2+}, (5) Cr^{2+}, (6) Co^{2+}, (7) Ni^{2+}, (8) Ag^{+}, (9) Fe^{2+}, (10) Pb^{2+}, (11) Al^{3+}, (12) Hg^{2+}, (13) Cd^{2+}, and (14) Zn^{2+}.

Time-resolved spectroscopic study

The inference drawn from steady-state spectroscopic experiments is further supported by the results of the fluorescence lifetime study. The lifetime (τ) is calculated for free ligand (**1**) and the ligand in presence of various metal ions using time-correlated single-photon count (TCSPC) experiment (Table S3 and Fig. S12, ESI†). The decay pattern of **1** is shown in Fig. 5a where the lifetime (τ) is found to be 1.48 ns. The decay pattern as well as the lifetime remains unaffected in the presence of various metal ions except Zn^{2+}. However, the addition of Zn^{2+} brings a noticeable change in the fluorescence decay pattern as demonstrated in Fig. 4a and b which is associated with an increase in the lifetime value to 3.24 ns. Such a small increase in the τ value could be justified from the change in the values of two parameters, the emissive rate of the fluorophore (Γ) and its rate of non-radiative decay to S_0 (k_{nr}), which in this case are acting in opposite directions.[72,73] The first one *i.e.* the radiative decay rate of **1** is increased upon

Zn^{2+} coordination as explained before and hence, leads to a lowering of the fluorescence lifetime. Chelation with Zn^{2+}, on the other hand, suppresses non-radiative decay pathways by rigidifying the flexible side arms which in turn results in an increase in the *τ* value of the system. These two opposing factors try to compensate each other and as a result the *τ* value could not be changed too much. However, the net increase in the lifetime value indicates that the second factor is dominating over the first one in this case. The observed bi-exponential decay in the presence of Zn^{2+} might be the outcome of the co-existence of two different species: one is the free ligand (**1**) with a shorter lifetime and the other is the Zn^{2+} adduct of **1** with a comparatively longer lifetime. Upon incremental addition of Zn^{2+} the contribution from the latter is increased and as a result a gradual increase in the lifetime is observed which is stopped after the addition of 3 equiv. of Zn^{2+} (Fig. 4b). This again supports the 1 : 3 binding stoichiometry between the host and guest as concluded from the steady state photophysical studies.

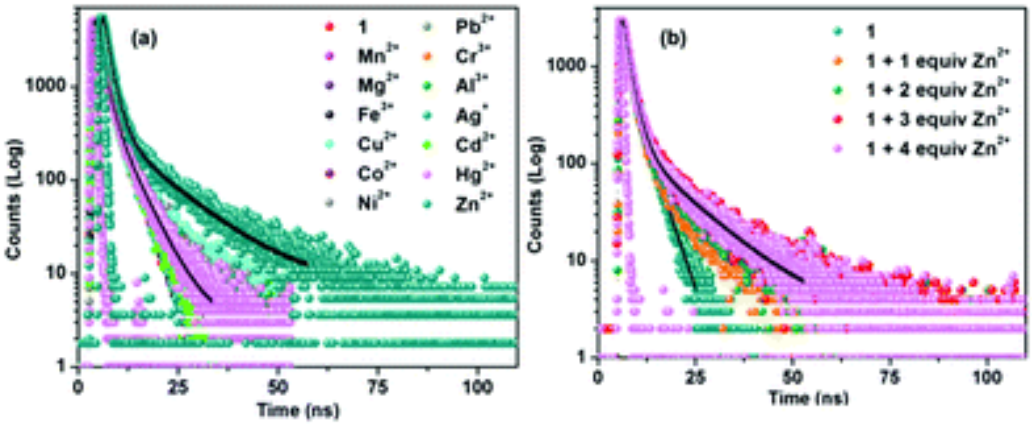

Fig. 4 Time-resolved luminescence decays of **1** (22.5×10^{-6} M; λ_{ex} = 340 nm and λ_{em} = 410 nm) (a) in the presence of various metal ions as their perchlorate salts and (b) upon the addition of an increasing amount of Zn^{2+} in acetonitrile at room temperature.

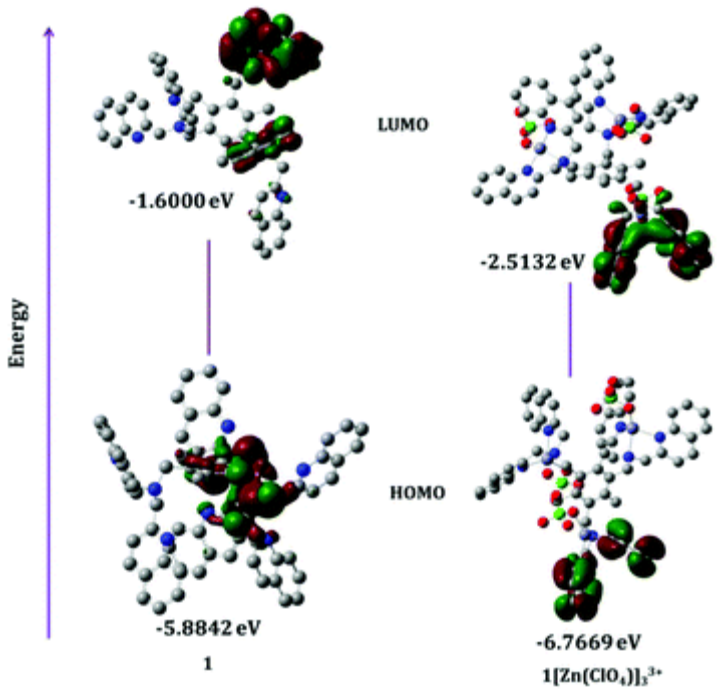

Fig. 5 Frontier molecular orbitals of **1** and **1**$[Zn(ClO_4)]_3^{3+}$ with their corresponding energy gaps as calculated from DFT B3LYP/6-31G(d) and the LanL2DZ mixed basis set. The 6-31G(d) basis set is used for H, C, N, O, and Cl atoms; Zn is treated with the LanL2DZ computational level using the IEFPCM model for acetonitrile [isovalue = 0.02].

^{1}H nuclear magnetic resonance spectroscopy and electrospray ionization mass spectrometry

From the previous section it is obvious that ligand **1** selectively binds the Zn^{2+} ion with 1 : 3 host–guest stoichiometry but the mode of interaction remains unrevealed. To know about this, a ^{1}H NMR titration experiment is carried out for **1** with Zn^{2+} in CD_3CN (Fig. S13, ESI†). Incremental addition of Zn^{2+} into **1** results in a gradual downfield shift of almost all quinoline protons as well as H_b and H_c, which are adjacent to the secondary N while the peak position corresponding to methyl protons (1.5 ppm) in the central arene ring (H_a) remains unaltered. However, the overall changes stopped after the addition of 3 equiv. of Zn^{2+}. This leads us to conclude that the quinoline nitrogens as well as the linker N simultaneously act as the donor site for chelation with the Zn^{2+} ion. Besides this, in the ESI-MS of the isolated Zn^{2+} complex of **1**, a peak is observed at 517.07 *m*/*z* which could be assigned for **1**$[Zn(ClO_4)]_3^{3+}$ with *m*/*z* 517.06 (Fig. S14, ESI†). The distribution patterns

of the species matches well with the corresponding theoretically calculated distribution patterns. Based on these, a possible structure of the zinc complex is outlined where three zinc ions are bound with the ligand and each of them coordinates with three nitrogens and one ClO_4^-. This approximated structure which is based on the ^1H NMR and ESI-MS studies agrees with all the solution state experimental outcomes as well as the previous reports.[74] According to this, a plausible mechanism is demonstrated in Scheme 2. Density functional theoretical (DFT) studies are performed to establish the proposed structure of the Zn^{2+} complex.

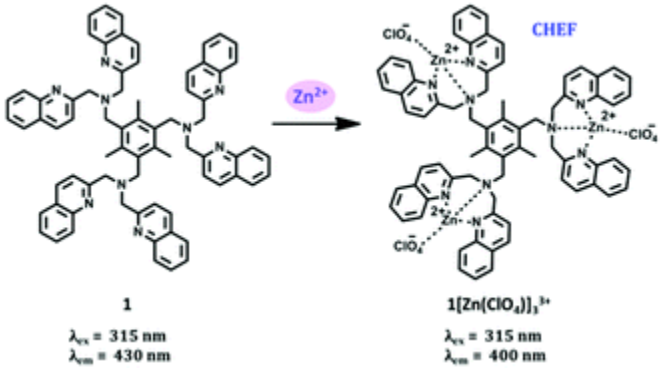

Scheme 2 Proposed binding mechanism of **1** with Zn^{2+} in acetonitrile.

Theoretical calculations for 1 and its Zn^{2+} complex

To investigate the stability and the structure–property relationship of the proposed zinc complex, DFT study is carried out on ground (S_0) and excited states (S_1) of both **1** and **1**$[Zn(ClO_4)]_3^{3+}$. The hybrid B3LYP functional[75] is used in all cases as integrated in the Gaussian 09 package,[76] mixing the exact Hartree–Fock-type exchange with the Becke's exchange functional[77] and that proposed by Lee–Yang–Parr for the correlation contribution.[78] The 6-31G(d)[79] basis set is used for C, N and H atoms and Zn is treated with LanL2DZ. The integral equation formalism variant of a polarizable continuum model (IEF-PCM)[80] is used to address the effect of acetonitrile (Fig. 5, Fig.

S15–S17 and Tables S4–S7, ESI†). The results reveal that, in acetonitrile the three side arms of the ligand are arranged in a propeller-like shape where three quinoline units are present on one side of the central arene ring while the other three are on the opposite side. As depicted in Fig. 5, upon the addition of Zn^{2+} the two quinoline rings in the same arm come closer to coordinate with Zn^{2+} resulting in a distorted tetrahedral geometry around it. Every Zn^{2+} ion is surrounded by two quinoline nitrogens, one secondary N and the O in a perchlorate anion. The corresponding bond lengths and bond angles are listed in Table S4, ESI.† From the energy level diagram shown in Fig. 5, it is obvious that the chelation of the ligand with Zn^{2+} does not induce a huge change in the value of energy difference between the HOMO and LUMO, instead a slight decrease in the same is observed. This agrees with the solution state photo-physical experimental finding indicating that the addition of Zn^{2+} does not lead to a remarkable shift in the absorption spectrum and only an increase in absorbance is observed in the presence of Zn^{2+}. The theoretically determined UV-vis spectra of the ligand as well as the proposed zinc complex match nicely with their corresponding absorption spectra which are observed in acetonitrile (Fig. S17 and Table S5, ESI†).

Zn^{2+} sensing by 1 in an aqueous medium

To check whether the ligand is capable to detect Zn^{2+} in an aqueous environment absorption and emission spectroscopic studies of **1** are carried out in an aqueous buffer (10 mM HEPES, pH 7.4)/CH_3CN (1 : 1 v/v) solvent mixture with various metal ions (*e.g.*, Mn^{2+}, Mg^{2+}, Cr^{3+}, Cu^{2+}, Cd^{2+}, Ag^{+}, Hg^{2+}, Al^{3+}, Pb^{2+}, Fe^{2+}, Ni^{2+}, Co^{2+} and Zn^{2+}). Two sharp absorption bands are observed at 303 nm (ε = 8580 M^{-1} cm^{-1}) and 315 nm (ε = 8411 M^{-1} cm^{-1}) in the UV-vis spectrum of the ligand, while the excitation at 315 nm results in an emission band at 430 nm with a small peak at 410 nm (Fig. 6a). Interestingly, the

emission intensity of **1** in aqueous buffer (10 mM HEPES, pH = 7.4) media is greater than the value observed in pure acetonitrile. The reason might be the hydrogen bonding interaction between quinoline nitrogens and water which decreases the electron density from nitrogens and consequently reduces the effect of the n–π* transition which was responsible for weakening the emission intensity in acetonitrile.[70,71]

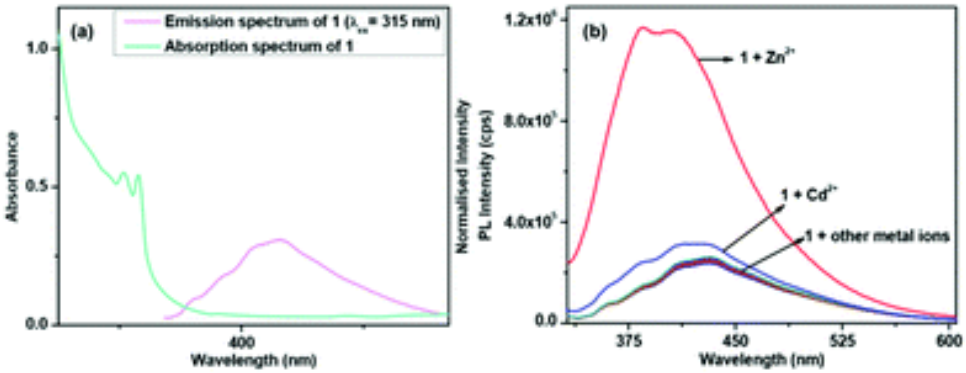

Fig. 6 (a) Absorption and emission profiles of **1** and (b) Emission spectrum of **1** in the presence of 10 equiv. various metal ions in an aqueous buffer (10 mM HEPES, pH 7.4)/acetonitrile (1 : 1 v/v).

The addition of an aqueous buffer solution of Zn^{2+} (10 equiv.) to the ligand leads to a luminescence color change from green to blue while the emission intensity increases up to 4.76 fold (Fig. 6b). The emission maximum shifts to a comparatively higher energy region to give two new peaks at 384 nm and 405 nm. The increase in the emission intensity in the presence of Zn^{2+} may be attributed to the rigidification of the side arms which leads an increase in the quantum efficiency. The presence of metal ions other than Zn^{2+} does not affect the emission profile significantly. For better understanding the zinc binding properties of **1** in aqueous buffer (10 mM HEPES, pH = 7.4) media, absorption and emission titration experiments are performed by the gradual addition of Zn^{2+} into an aqueous buffer (10 mM HEPES, pH 7.4)/acetonitrile (1 : 1 v/v) solution of **1**. Upon the addition of an increasing amount of Zn^{2+}, a gradual increase in the absorbance of the

bands at 303 nm and 315 nm is observed with the appearance of a single isosbestic point at 280 nm (Fig. S18, ESI†). In an emission titration experiment, the addition of Zn^{2+} results in a blue shift of the emission bands from 430 and 410 nm to 384 and 405 nm, respectively, with a steady increase in the emission intensity. The saturation point is reached at 3 equiv. Zn^{2+} concentration which along with the corresponding Job plot analysis reveals 1 : 3 stoichiometric binding between **1** and Zn^{2+} (Fig. 7a and b). The binding constant between **1** and Zn^{2+} is found to be K_{Zn1} = 1.27 × 10^4, K_{Zn2} = 9.55 × 10^3 and K_{Zn3} = 6.89 × 10^3 M^{-1} (Fig. 7c) and the calibration curve of change in emission intensity ($I - I_0$) *versus* the concentration of Zn^{2+} results in the detection limit 29.45 × 10^{-8} M (Fig. S19a, ESI†). The selectivity of the ligand toward Zn^{2+} is also studied by monitoring the change in the emission spectrum of **1** upon the addition of 3 equiv. Zn^{2+} in the presence of various metal ions (10 equiv. each) in an aqueous buffer (10 mM HEPES, pH 7.4)/acetonitrile (1 : 1 v/v) solution. The result shows almost the same emission spectral changes in each case as observed with only Zn^{2+} in the absence of other metal ions (Fig. S19b, ESI†). However, no remarkable change is observed in the fluorescence decay profile of **1** upon the addition of an incremental concentration of Zn^{2+} in its aqueous buffer (10 mM HEPES, pH 7.4)/acetonitrile (1 : 1 v/v) solution (Fig. S20, ESI†). This indirectly suggests that the extent of the increase in the lifetime by reducing the probability of non-radiative decay *via* rigidification of the flexible ligand upon zinc coordination might be just comparable to the effect of lowering the τ value due to the increase in the emissive rate of the fluorophore as explained before. Thus the two opposite factors completely compensate each other resulting in no change in the lifetime value.

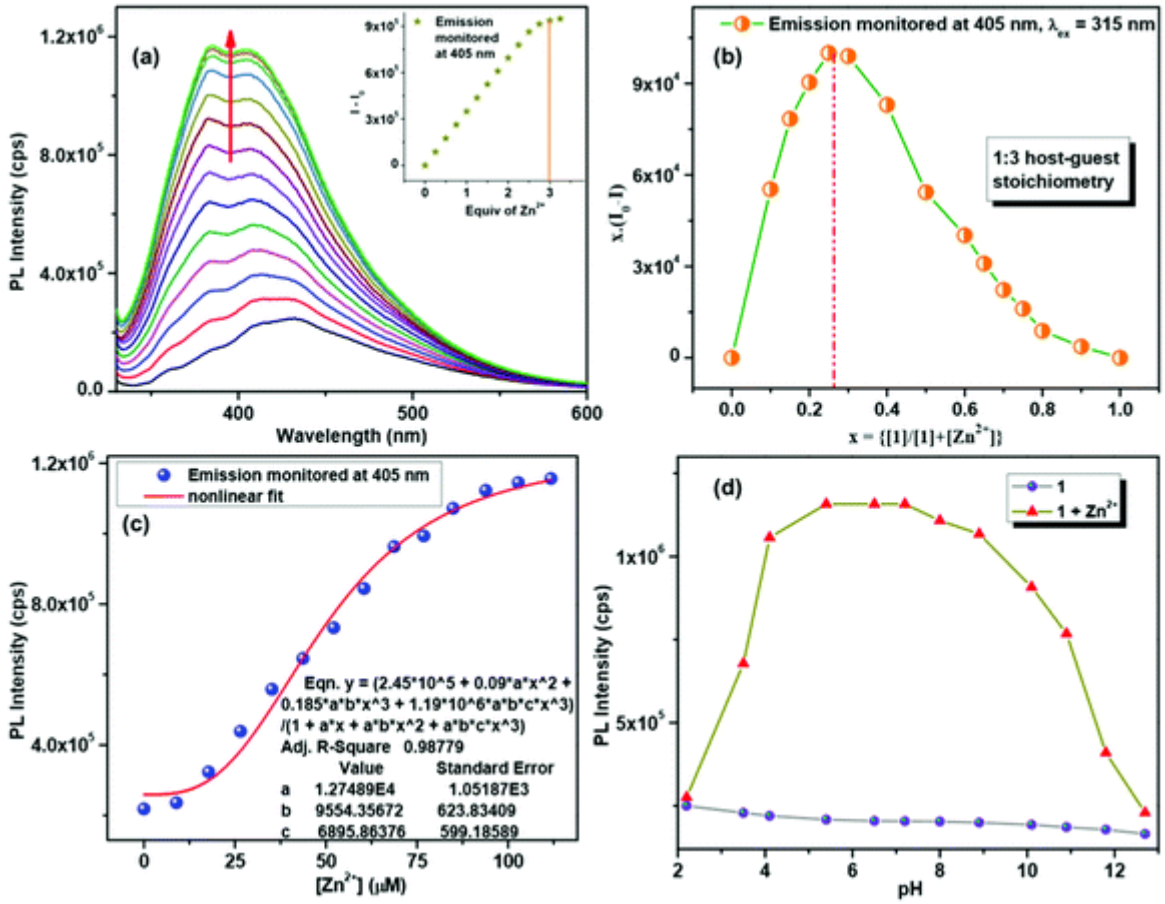

Fig. 7 (a) Emission titration profile of **1** (10×10^{-6} M) with Zn^{2+} (Inset: Corresponding equivalent plot) and (b) PL Job plot experiment of **1** (15×10^{-6} M) with Zn^{2+} (15×10^{-6} M) in an aqueous buffer (10 mM HEPES, pH 7.4)/acetonitrile (1 : 1 v/v); (c) non-linear 1 : 3 fitting of the PL titration data to calculate an association constant of **1** with Zn^{2+} in an aqueous buffer (10 mM HEPES, pH 7.4)/acetonitrile (1 : 1 v/v) at room temperature. (d) Emission intensity of **1** and **1** in the presence Zn^{2+} at a different pH.

Effect of pH on Zn^{2+} sensing by 1.

Since pH is one of the major factors governing the practical application of a sensor in the sensing of environmental as well as biological samples, the effect of pH upon the Zn^{2+} sensing properties of **1** is duly investigated. For all the above mentioned sensing studies in an aqueous buffer (10 mM HEPES, pH = 7.4) solvent, the pH of the solution remains the same before and after the addition of Zn^{2+}. This justifies the fact that the changes observed in the spectral properties of **1** upon the addition of Zn^{2+} are exclusively

due to its coordination with Zn^{2+} but not for the effect of pH. Changing the pH from 4 to 10 does not lead to any significant change in the emission intensity value of the free ligand while the extent of emission enhancement in the presence of 3 equiv. Zn^{2+} is reduced at a highly acidic or basic pH *i.e.* it stops beyond pH 4 on acidic side and pH 10 on basic side (Fig. 7d). The decrease in the sensing efficiency of **1** at highly acidic pH might be the result of protonation on quinoline nitrogens, which traps the nonbonding electron pairs on N, through which it could coordinate with the metal. Though the PET from nitrogen centers is stopped the occurrence of non-radiative decay is not inhibited because of the flexibility in the side arm in the absence of Zn^{2+}. On the other hand, at a highly basic pH, a competition starts between the ligand and OH^- ion for binding with Zn^{2+} which lowers the sensitivity of **1** toward Zn^{2+}.[18] Thus, it can be concluded from the overall experimental results that **1** can be used as a selective fluorescent sensor for Zn^{2+} in acetonitrile as well as in 50% aqueous buffer (10 mM HEPES, pH = 7.4) acetonitrile system.

Single crystal X-ray structural analysis of the Zn^{2+} complex

To get the solid state structural evidence of Zn^{2+} binding with **1**, X-ray structural analysis is performed with the single crystals of the resulting zinc complex obtained from the slow evaporation of its DMF/methanol/water (3 : 1 : 1) solution. The complex crystallizes in the $P2_1$ space group where the asymmetric unit contains the ligand, three Zn^{2+} ions, three ClO_4^-, three NO_3^- groups and the solvent molecules (Table S8, ESI†). Interestingly, the 1 : 3 ligand–metal stoichiometry which has already been observed in detailed solution state studies is further assisted by the single crystal X-ray structure. As depicted in Fig. S21,† every Zn^{2+} ion is chelated with **1***via* two quinoline nitrogens and one secondary nitrogen atom. One nitrate bridges two Zn^{2+} centers leading to a different

coordination number and geometry around them *i.e.* one is pentacoordinated while the other one is tetracoordinated. The remaining zinc centre binds with two oxygen atoms from the solvent molecules to adopt a pentacoordinated geometry.

Anion sensing by the trinuclear Zn^{2+} complex. High aqueous solubility of the trinuclear Zn^{2+} complex and presence of NO_3^- in the coordination sphere insists us to check whether it can be replaced by other anions. To see this, the change in the emission spectral behavior of the complex is monitored in the presence of various anions as their sodium salts in a 70% aqueous buffer (10 mM HEPES, pH = 7.4) acetonitrile solution. The addition of an excess amount (20 equiv.) of different anions like F^-, Cl^-, Br^-, $HCOO^-$, CH_3COO^-, ClO_4^-, SO_4^{2-}, $H_2PO_4^-$, AMP and ADP does not cause any appreciable change in the emission spectrum of the complex while in the presence of 5 equiv. of PPi the emission intensity is decreased drastically (Fig. 8). Excess ATP (20 equiv.) also reduces the intensity but to a small extent. However, the quenching of emission intensity in the presence of PPi is not perturbed even in the presence of excess ATP in the medium. Careful analysis of the single crystal X-ray structure of the Zn^{2+} complex, described above, reveals that two Zn^{2+} centres are separated by 4.639 Å which matches very well with that of the length of a PPi anion. This analogy suggests the probable reason behind the selectivity toward PPi, which is, the best fitting of the guest between two Zn^{2+} centres. For other structurally similar phosphate analogues this fitting does not occur efficiently resulting in a silent behavior of the trinuclear Zn^{2+} complex towards these anions.

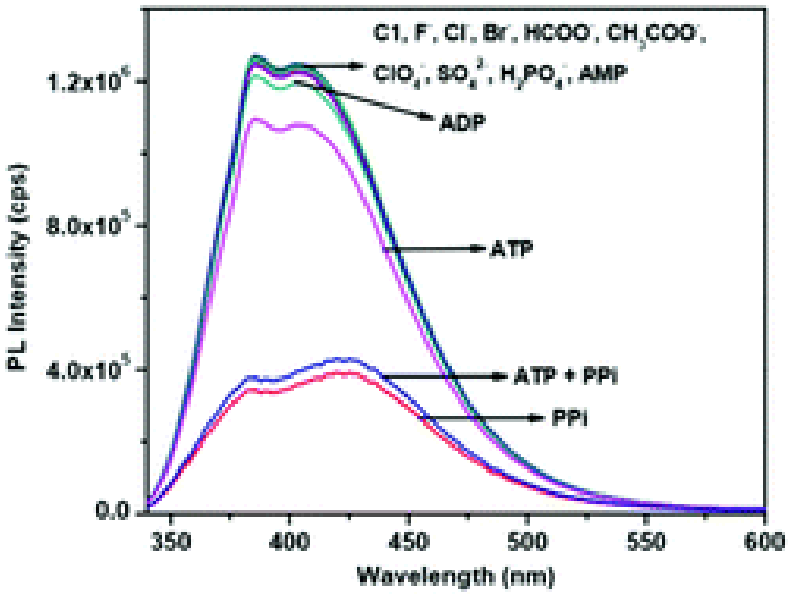

Fig. 8 Emission spectral changes of the trinuclear Zn^{2+} complex (8.5×10^{-6} M) in the presence of various anions (5 equiv. PPi and 20 equiv. other anions) as their sodium salts, in 70% aqueous buffer (10 mM HEPES, pH = 7.4) acetonitrile at room temperature.

To know the PPi binding better, the emission titration experiment of the trinuclear Zn^{2+} complex with PPi is carried out. It shows a gradual decrease in emission intensity upon incremental addition of PPi (Fig. 9a) where the changes are ceased beyond the addition of 2 equiv. of the anion (Fig. 9b). The results along with the PL Job plot (Fig. S22a, ESI†) suggest 1 : 2 host–guest stoichiometry while the detection limit is calculated to be 45.37×10^{-9} M (Fig. 9c) and the related association constants are determined by a nonlinear curve fitting method as 5.03×10^5 and 1.84×10^5 M^{-1} (Fig. S22b, ESI†). The values suggest a very high sensitivity as well as a significant binding efficiency of the trinuclear Zn^{2+} complex toward PPi which is good enough when compared with those of previously reported PPi sensors (Table S10, ESI†). The selectivity study shows that the quenching of the fluorescence upon the addition of a PPi anion remains unperturbed even in the presence of other competitive anions (Fig. 9d). Based on the experimental outcomes, pieces of spectroscopic evidence (Fig. S23, ESI†), and previous literature reports,[19,24] a probable binding mode is demonstrated in Scheme S1, ESI,† where two PPi anions form an adduct with the trinuclear Zn^{2+} complex. The NO_3^- anion which was bridged between two Zn^{2+} ions is replaced by one PPi while the other PPi coordinates

with the third Zn^{2+}. Thus, as depicted in Scheme S1, ESI,† every Zn^{2+} ion adopts five-coordination mode. The quenching of the emission intensity of the trinuclear Zn^{2+} complex in the presence of PPi could be attributed to the weakening of the N → Zn bond upon the coordination of the Zn^{2+} ions with a PPi anion.[19,24] This effectively increases the density of the non-bonding electrons over quinoline nitrogens, which, as discussed in the previous section, favors the ISC process from n–π* singlet → n–π* triplet and as a result the luminescence of the system is quenched. Thus, the decrease of the emission intensity upon the addition of a very small amount (only 2 equiv.) of PPi makes the trinuclear Zn^{2+} complex a suitable "turn-OFF" fluorescence sensor for PPi in 70% aqueous buffer (10 mM HEPES, pH = 7.4) acetonitrile media.

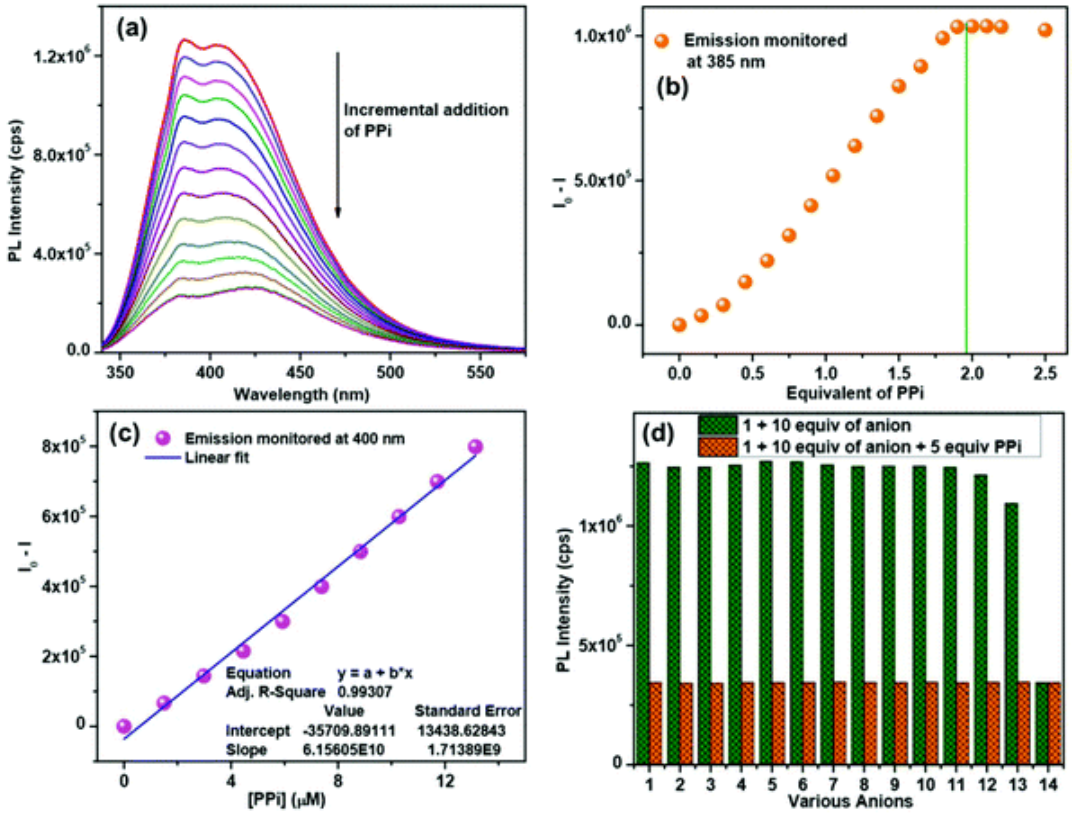

Fig. 9 (a) Emission titration profile of the trinuclear Zn^{2+} complex (10 μM) with PPi, (b) corresponding equivalent plot, (c) the corresponding calibration curve and (d) selectivity graph of the trinuclear Zn^{2+} complex with PPi in the presence of other metal ions in a 70% aqueous buffer (10 mM HEPES, pH 7.4)/acetonitrile media at room temperature (λ_{em} = 385 nm). Green bars represent the fluorescence intensities in the presence of other anions (10 equiv.) and the red bars correspond to the same in the presence of all anions and PPi. Codes used: (1) trinuclear Zn^{2+} complex, (2) F^-, (3) Cl^-, (4) Br^-, (5) $HCOO^-$, (6) CH_3COO^-, (7) HCO_3^-, (8) ClO_4^-, (9) SO_4^{2-}, (10) $H_2PO_4^-$, (11) AMP, (12) ADP, (13) ATP, and (14) PPi.

Conclusions

In summary, an efficient quinoline based highly sensitive C_3-symmetric fluorescent sensor is developed that can discriminate Zn^{2+} among various competitive metal ions including Cd^{2+} even in a 50% aqueous buffer medium. The solution state experimental results and DFT calculations suggest the formation of a trinuclear Zn^{2+} complex which is further confirmed by the ingle crystal X-ray diffraction study. The solid state structure shows that a NO_3^- group is bridged between two Zn^{2+} centers in the complex which in turn, shows selective fluorescence “turn-OFF” sensing of PPi in a 70% aqueous buffer (10 mM HEPES, pH = 7.4) acetonitrile medium.

Experimental

Materials

All the reaction and workup procedures were carried out under ambient conditions. 2-(Chloromethyl)quinoline hydrochloride, potassium iodide, and the perchlorate salts of Zn^{2+}, Cd^{2+}, Hg^{2+}, Pb^{2+}, Fe^{2+}, Ni^{2+}, Co^{2+}, Al^{3+}, Cr^{3+}, Cu^{2+}, Mg^{2+}, Ag^{+} and Mn^{2+} and sodium salts of the anions were purchased from Sigma-Aldrich and used as received. Potassium carbonate and the nitrate salt of Zn^{2+} were bought from Merck chemicals. Ethanol and acetonitrile solvents were purchased from Spectrochem Pvt. Ltd, India. All of them were used as received except acetonitrile which was further dried and distilled using CaH_2. HPLC-grade solvents and doubly distilled water were used in photophysical measurements. NMR solvents were purchased from Sigma-Aldrich.

Methods

Fourier transform infrared (FTIR) spectra were recorded on a Shimadzu FTIR-8400S infrared spectrophotometer with KBr pellets. High-resolution mass spectrometry (HRMS) analyses were carried out using a QTOF–Micro YA 263 mass spectrometer in positive ESI mode. ^{1}H, ^{13}C, $^{1}H–^{1}H$ COSY, ^{1}H-DEPT-135 HSQC and $^{1}H–^{13}C$ HMBC NMR experiments were carried out on a FT-NMR Bruker DPX 300/400/500 MHz NMR spectrometer, and the chemical shift values for ^{1}H and ^{13}C NMR were reported in parts per million (ppm), calibrated to the residual solvent peak set. Absorption spectra were recorded on a PerkinElmer Lambda 900 UV/vis/NIR spectrometer using a quartz cuvette of 1 cm path length whereas the emission spectra were recorded in a FluoroMax-3 spectrophotometer, from Horiba Jobin Yvon. Elemental analysis was performed on a PerkinElmer 2500 series II elemental analyzer, PerkinElmer, USA. A picosecond diode laser (IBH Nanoled-07) was used to excite the samples in an IBH Fluorocube apparatus for TCSPC measurements. The luminescence decays were recorded on a Hamamatsu MCP photomultiplier (R3809), and the analysis of the data was done using the IBH DAS6 software. All geometry optimizations were performed with the Gaussian 09[76] program package using DFT. The B3LYP[75] functional was used with the 6-31G(d) basis set[79] for C, N, H and LanL2DZ for Zn atoms. An integral equation formalism variant of the Polarizable continuum model (IEF-PCM)[80] was employed to include the solvent (acetonitrile) effect. Time-dependent DFT calculations were done to characterize the peaks in the excitation spectrum. Gaussview 5.0 was used for visualizations of the optimized structures and the MOs. Caution: Metal perchlorate salts are explosive in the presence of open flames, heat or sparks. Zinc perchlorate hexahydrate and zinc nitrate hexahydrate can cause skin and eye damage. All due precautions should be taken while handling these.

Calculation of association constants. The 1 : 3 association constants were determined using a nonlinear least-squares analysis of *I versus* c_M using the deduced equation:[81a]

$$I = \frac{I_0 + c_M \Phi_1 K_{11}[\mathrm{M}] + c_M \Phi_1 \beta_{21}[\mathrm{M}]^2 + I_{\mathrm{lim}} \beta_{31}[\mathrm{M}]^3}{1 + K_{11}[\mathrm{M}] + \beta_{21}[\mathrm{M}]^2 + \beta_{31}[\mathrm{M}]^3}$$

where $\beta_{21} = K_{11}K_{21}$, $\beta_{31} = K_{11}K_{21}K_{31}$, and [M] ≈ c_M are the concentrations of Zn^{2+} ions, I_0 or I is integrated emission in the absence or presence of Zn^{2+}. Φ_1 is approximately 0.09, the quantum yield of the 1 : 1 **1**-Zn^{2+} complex; Φ_2 is approximately 0.185, the quantum yield of the 1 : 2 **1**-Zn^{2+} complex.

The 1 : 2 association constants between the trinuclear Zn^{2+} complex and PPi are determined by using the equation:[81b]

$$\Delta I = \frac{\Phi_1 K_{11}[\mathrm{H}]_0[\mathrm{G}] + \Phi_2 K_{11}[\mathrm{H}]_0[\mathrm{G}]^2}{1 + K_{11}[\mathrm{G}] + K_{11}K_{21}[\mathrm{G}]^2}$$

where [G] ≈ the concentration of the trinuclear Zn^{2+} complex Φ_1 is approximately 0.185, the quantum yield of the 1 : 1 Zn^{2+} complex-PPi species; Φ_2 is approximately 0.09, the quantum yield of the 1 : 2 Zn^{2+} complex-PPi species.

Calculation of detection limit. Detection limits (DL) were calculated using the following equation:

$$\mathrm{DL} = (3 \times \mathrm{SD})/\mathrm{slope}$$

where SD corresponds to the standard deviation of the blank sample, measured using 15 consecutive scans of the blank sample. The slope is obtained from the linear fit plot of PL intensity changes *versus* the concentration of Zn^{2+} added. The SD values of ligand **1** were 1000.46 in acetonitrile and 995.59 in an aqueous buffer (10 mM HEPES, pH 7.4)/acetonitrile (1 : 1 v/v). In the case of a trinuclear Zn^{2+} complex the value was 930.99.

Calculation of excited-state lifetimes. The following equation was used to analyze the time-resolved emission decays:

$$P(t) = B + \sum_i \alpha_i e^{-t/\tau_i}$$

where $P(t)$ is decay, i is the number of discrete emissive species, B is the baseline correction, α_i is the pre-exponential factor, and τ_i is the excited state lifetime associated with the i^{th} component. In the case of multi-exponential decays the following equation was used to calculate an average lifetime:

$$\langle \tau \rangle = \sum_i \alpha_i \tau_i$$

where a_i is the contribution of the i^{th} decay component, and $a_i = \alpha_i / \Sigma \alpha_i$.

X-ray crystallographic refinement details for 1 and Zn^{2+} complex. In each case, a diffractable size crystal was collected from the mother liquor, dipped in paratone oil, and then it was cemented on the tip of a glass fiber using an epoxy resin. The intensity data of the crystals were collected using Mo Kα (λ = 0.7107 Å) radiation on a Bruker SMART APEX diffractometer, equipped with a CCD area detector at 100 K and 106 K for **1** and its tri-nuclear Zn^{2+} complex, respectively. Data integration and reduction were processed by the SAINT[82a] software. Empirical absorption correction to the collected reflections was done by applying SADABS.[82b] The structures were solved using SHELXTL[83] and was refined on F2 by the full-matrix least-squares technique using the SHELXL-97[84] program package. PLATON-97[85] and MERCURY 3.8[86] were used to generate graphics. Some of the carbon and nitrogen atoms of one quinoline ring in **1** and the trinuclear Zn^{2+} complex are highly disordered. Some other disordered solvent molecules are removed using the PLATON/SQUEEZE program. The occupancy factors of the disordered atoms are refined using the FVAR command of the SHELXTL program and are isotropically refined. Though good crystals have been selected and the data have been collected at 150 K,

the crystals did not show diffraction beyond the theta max 20.39 and 20.81 for **1** and trinuclear Zn^{2+} complex, respectively, even after several data collections. CCDC 1583646 and 1583647† contain the supplementary crystallographic data for this paper.

Synthesis

1,3,5-Tris (aminomethyl)-2,4,6-trimethylbenzene was prepared as per the modified literature procedure where 1,3,5-tris(bromomethyl)-2,4,6-trimethyl benzene is used instead of 1,3,5-tris(bromomethyl)-2,4,6-triethyl benzene.[44]

Synthesis of *N,N′,N″*-((2,4,6-trimethylbenzene-1,3,5-triyl)tris(methylene))tris(1-(quinolin-2-yl)-*N*-(quinolin-2 ylmethyl)methanamine) (1). A mixture of 2-(chloromethyl)quinoline hydrochloride (6.634 g, 31 mmol) and K_2CO_3 (9.674 g, 70 mmol) in 15 mL acetonitrile was stirred at room temperature for 5 minutes. Then 1,3,5-tris(aminomethyl)-2,4,6-trimethylbenzene[44] (1.035 g, 5 mmol) and a pinch amount of KI were added to it. The reaction mixture was refluxed and stirred for 12 h. After that the remaining acetonitrile was evaporated and the resulting residue was extracted in dichloromethane (DCM). The DCM part was evaporated to get an ash-colored crude product which was further purified by column chromatography with silica gel of a 60–120 mesh size using chloroform/methanol as an eluent. The pale yellow-brown colored desired product was obtained with 70% yield (3.68 g) at 10% methanol concentration. Elemental analysis: calcd (%) for $C_{72}H_{63}N_9$: C, 82.02; H, 6.02; N, 11.96. Found: C, 81.96; H, 6.14; N, 11.76. FTIR in a KBr disc (ν/cm^{-1}): 3404, 3057, 2922, 2873, 1599, 1564, 1502, 1425, 1381, 1367, 1309, 1223, 1117, 978, 949, 829, 764, 671, 619. ESI-MS $[C_{72}H_{63}N_9][H^+]$ calcd: *m*/*z* 1054.33. Found: *m*/*z* 1054.51. ^{1}H NMR (300 MHz, $CDCl_3$, $Si(CH_3)_4$): δ 7.977 (d, J = 8.4 Hz, 6H, H_i), 7.813 (d, J = 8.4 Hz, 6H, H_e), 7.627 (t, J = 8.4

Hz, 6H, H_h), 7.575 (d, *J* = 8.4 Hz, 6H, H_f), 7.412 (t, *J* = 8.4 Hz, 6H, H_g), 7.310 (d, *J* = 8.4 Hz, 6H, H_d), 3.882 (s, 12H, H_c), 3.748 (s, 6H, H_b), 2.267 (s, 9H, H_a). ^{13}C NMR (125 MHz, $CDCl_3$, $Si(CH_3)_4$): *δ* 160.33 (6C, C_m), 147.41 (6C, C_l), 138.28 (6C, C_j), 136.16 (6C, C_e), 133.19 (6C, C_n), 129.50 (6C, C_h), 129.05 (6C, C_i), 127.44 (12C, $C_{f,k}$), 61.34 (12C, C_c), 53.50 (6C, C_b), 17.06 (9C, C_a).

Conflicts of interest

There are no conflicts to declare.

Acknowledgements

P. G. gratefully acknowledges the Science and Engineering Research Board (SERB; EMR/2016/000900), India, for financial support and the Alexander von Humboldt Foundation for donating a fluorometer. S. S. would like to thank CSIR, India, for SRF.

References

1. Z. Xu, J. Yoon and D. R. Spring, Chem. Soc. Rev., 2010, 39, 1996–2006 RSC.
2. Z. Xu, K.-H. Baek, H. N. Kim, J. Cui, X. Qian, D. R. Spring, I. Shin and J. Yoon, J. Am. Chem. Soc., 2010, 132, 601–610
3. C. Rivas, G. J. Stasiuk, M. S. Henga and N. J. Long, Dalton Trans., 2015, 44, 4976–4985 RSC.
4. S. Zhang, R. Adhikari, M. Fang, N. Dorh, C. Li, M. Jaishi, J. Zhang, A. Tiwari, R. Pati, F.-T. Luo and H. Liu, ACS Sens., 2016, 1, 1408–1415
5. X. Yan, J. J. Kim, H. S. Jeong, Y. K. Moon, Y. K. Cho, S. Ahn, S. B. Jun, H. Kim and Y. You, Inorg. Chem., 2017, 56, 4332–4346
6. L. Yan, R. Li, F. Ma and Z. Qi, Anal. Methods, 2017, 9, 1119–1124 RSC .
7. (a) M. Shyamal, P. Mazumdar, S. Maity, S. Samanta, G. P. Sahoo and A. Misra, ACS Sens., 2016, 1, 739–747; (b) S. Goswami, S. Paul and A. Manna, Tetrahedron Lett., 2014, 55, 3946–3949; (c) A. Manna, K. Jana, N. Guchhait and S. Goswami, New J. Chem., 2017, 41, 6661–6666 RSC .
8. (a) Y. Dong, R. Fan, W. Chen, P. Wang and Y. Yang, Dalton Trans., 2017, 46, 6769–6775 RSC ; (b) S. Goswami, A. Manna, S. Paul, K. Aich, A. K. Das and S. Chakraborty, Dalton Trans., 2013, 42, 8078–8085 RSC ; (c) S. Goswami, S. Paul and A. Manna, RSC Adv., 2013, 3, 10639–10643 RSC .

9. B. A. Wong, S. Friedle and S. J. Lippard, J. Am. Chem. Soc., 2009, 131, 7142–7152 CrossRef CAS
10. H. G. Lee, J. H. Lee, S. P. Jang, I. H. Hwang, S. J. Kim, Y. Kim, C. Kim and R. G. Harrison, Inorg. Chim. Acta, 2013, 394, 542–551 .
11. E. Hao, T. Meng, M. Zhang, W. Pang, Y. Zhou and L. Jiao, J. Phys. Chem. A, 2011, 115, 8234–8241
12. K. P. Carter, A. M. Young and A. E. Palmer, Chem. Rev., 2014, 114, 4564–4601
13. H. Mehdi, H. Pang, W. Gong, A. Wajahat, K. D. Manivannan, S. Shah, J. Ye and G. Ning, Supramol. Chem., 2017, 29, 378–386 .
14. S. Majumder, L. Mandal and S. Mohanta, Inorg. Chem., 2012, 51, 8739–8749
15. L. Xue, H.-H. Wang, X.-J. Wang and H. Jiang, Inorg. Chem., 2008, 47, 4310–4318
16. X. Zhang, D. Hayes, S. J. Smith, S. Friedle and S. J. Lippard, J. Am. Chem. Soc., 2008, 130, 15788–15789
17. S. C. Burdette, G. K. Walkup, B. Spingler, R. Y. Tsien and S. J. Lippard, J. Am. Chem. Soc., 2001, 123, 7831–7841
18. B. Chowdhury, R. Dutta, S. Khatua and P. Ghosh, Inorg. Chem., 2016, 55, 259–271
19. K. K. Sook, D. H. Lee, J. I. Hong and J. Yoon, Acc. Chem. Res., 2009, 42, 23–31
20. S. Xu, M. He, H. Yu, X. Cai, X. Tan, B. Lu and B. Shu, Anal. Biochem., 2001, 299, 188–193
21. W. N. Lipscomb and N. Straeter, Chem. Rev., 1996, 96, 2375–2434
22. P. Das, N. B. Chandar, S. Chourey, H. Agarwalla, B. Ganguly and A. Das, Inorg. Chem., 2013, 52, 11034–11041
23. J. L. Sessler, J. Cai, H. Y. Gong, X. Yang, J. F. Arambula and B. P. Hay, J. Am. Chem. Soc., 2010, 132, 14058–14060 PubMed ; S. Lee, K. K. Y. Yuen, K. A. Jolliffe and J. Yoon, Chem. Soc. Rev., 2015, 44, 1749–1762 RSC .
24. B. Chowdhury, S. Sinha and P. Ghosh, Chem. – Eur. J., 2016, 22, 18051–18059
25. J. Hatai, S. Pal and S. Bandyopadhyay, Tetrahedron Lett., 2012, 53, 4357–4360
26. J. P. Anzenbacher, M. A. Palacios, K. Jursíková and M. Marquez, Org. Lett., 2005, 7, 5027–5030
27. S. Nishizawa, Y. Kato and N. Teramae, J. Am. Chem. Soc., 1999, 121, 9463–9464
28. B. K. Datta, S. Mukherjee, C. Kar, A. Ramesh and G. Das, Anal. Chem., 2013, 85, 8369–8375
29. Y. Mikata, A. Kizu, K. Nozaki, H. Konno, H. Ono, S. Mizutani and S. Sato, Inorg. Chem., 2017, 56, 7404–7415
30. X. J. Jiang, M. Li, H. L. Lu, L. H. Xu, H. Xu, S. Q. Zang, M. S. Tang, H. W. Hou and T. C. W. Mak, Inorg. Chem., 2014, 53, 12665–12667
31. K. Aich, S. Goswami, S. Das, C. Das Mukhopadhyay, C. K. Quah and H.-K. Fun, Inorg. Chem., 2015, 54, 7309–7315
32. L. Xue, G. Li, Q. Liu, H. Wang, C. Liu, X. Ding, S. He and H. Jiang, Inorg. Chem., 2011, 50, 3680–3690
33. C. Lu, Z. Xu, J. Cui, R. Zhang and X. Qian, J. Org. Chem., 2007, 72, 3554–3557
34. Y. Mikata, K. Kawata, S. Iwatsuki and H. Konno, Inorg. Chem., 2012, 51, 1859–1865
35. L. Xue, G. Li, D. Zhu, Q. Liu and H. Jiang, Inorg. Chem., 2012, 51, 10842–10849
36. P. Du and S. J. Lippard, Inorg. Chem., 2010, 49, 10753–10755
37. E. M. Nolan and S. J. Lippard, Acc. Chem. Res., 2009, 42, 193–203
38. L. Xue, Q. Liu and H. Jiang, Org. Lett., 2009, 11, 3454–3457
39. S. Huang, R. J. Clark and L. Zhu, Org. Lett., 2007, 9, 4999–5002

40. H. Liua, Y. Dongc, B. Zhanga, F. Liua, C. Tana, Y. Tana and Y. Jianga, Sens. Actuators, B, 2016, 234, 616–624
41. Y. Fu, C. Fan, G. Liu, S. Cui and S. Pu, Dyes Pigm., 2016, 126, 121–130
42. (a) Y. Zhang, X. Guo, W. Si, L. Jia and X. Qian, Org. Lett., 2008, 10, 473–476 PubMed ; (b) C. He, Z. Lin, Z. He, C. Duan, C. Xu, Z. Wang and C. Yan, Angew. Chem., Int. Ed., 2008, 47, 877–881
43. E. M. Nolan, J. Jaworski, K.-I. Okamoto, Y. Hayashi, M. Sheng and S. J. Lippard, J. Am. Chem. Soc., 2005, 127, 16812–16823
44. I. Ravikumar and P. Ghosh, Inorg. Chem., 2011, 50, 4229–4231
45. D. Maity and T. Govindaraju, Chem. Commun., 2012, 48, 1039–1041 RSC .
46. S. Sreejith, K. P. Divya and A. Ajayaghosh, Chem. Commun., 2008, 2903–2905 RSC .
47. H. Kim, J. Kang, K. B. Kim, E. J. Song and C. Kim, Spectrochim. Acta, Part A, 2014, 118, 883–887
48. A. K. Bhanja, C. Patra, S. Mondal, D. Ojha, D. Chattopadhyay and C. Sinha, RSC Adv., 2015, 5, 48997–49005 RSC .
49. Y. Zhou, Z. X. Li, S. Q. Zang, Y. Y. Zhu, H. Y. Zhang, H. W. Hou and T. C. W. Mak, Org. Lett., 2012, 14, 1214–1217
50. F. Sun, G. Zhang, D. Zhang, L. Xue and H. Jiang, Org. Lett., 2011, 13, 6378–6381
51. W.-H. Chen, Y. Xing and Y. Pang, Org. Lett., 2011, 13, 1362–1365
52. (a) D. Juoh, M. Suhan and K. H. Ahn, Supramol. Chem., 2007, 19, 315–320; (b) X. Liu, P. Du and R. Cao, Nat. Commun., 2013, 4, 2375; (c) Z. Li, X.-H. Yu, Y. Chen, D.-Q. Yuan and W.-H. Chen, J. Org. Chem., 2017, 82, 13368–13375 ; (d) J. Wanga, X. Liua and P. Pan, J. Mater. Chem. B, 2014, 2, 6634–6638 RSC
53. R. R. Zhao, Q. L. Xu, Y. Yang, J. Cao, Y. Zhou, R. Xu and J. F. Zhang, Tetrahedron Lett., 2016, 57, 5022–5025
54. D. H. Lee, S. Y. Kim and J.-I. Hong, Angew. Chem., Int. Ed., 2004, 43, 4777–4780
55. S. Khatua, S. H. Choi, J. Lee, K. Kim, Y. Do and D. G. Churchill, Inorg. Chem., 2009, 48, 2993–2999
56. J. F. Zhang, S. Kim, J. H. Han, S.-J. Lee, T. Pradhan, Q.-Y. Cao, S.-J. Lee, C. Kang and J.-S. Kim, Org. Lett., 2011, 13, 5294–5297
57. B. Naskar, R. Modak, D. K. Maiti, M. G. B. Drew, A. Bauzá, A. Frontera, C. Das Mukhopadhyay, S. Mishra, K. Das Sahae and S. Goswami, Dalton Trans., 2017, 46, 9498–9510 RSC .
58. H. K. Cho, D. H. Leea and J.-I. Hong, Chem. Commun., 2005, 1690–1692 RSC .
59. S. Bhowmik, B. Ghosh, V. Marjomaki and K. Rissanen, J. Am. Chem. Soc., 2014, 136, 5543–5546
60. M. An, B.-Y. Kima, H. Seo, A. Helal and H. S. Kim, Spectrochim. Acta, Part A, 2016, 169, 87–94
61. O. G. Tsay, S. T. Manjare, H. Kim, K. M. Lee, Y. S. Lee and D. G. Churchill, Inorg. Chem., 2013, 52, 10052–10061
62. S. Anbu, S. Kamalraj, C. Jayabaskaran and P. S. Mukherjee, Inorg. Chem., 2013, 52, 8294–8296
63. K. Kim, Y. Ha, L. Kaufman and D. G. Churchill, Inorg. Chem., 2012, 51, 928–938
64. A. Gogoi and G. Das, RSC Adv., 2014, 4, 55689–55695 RSC .
65. B. Roy, A. S. Rao and K. H. Ahn, Org. Biomol. Chem., 2011, 9, 7774–7779

66. S. Lohar, S. Pal, M. Mukherjee, A. Maji, N. Demitri and P. Chattopadhyay, RSC Adv., 2017, 7, 25528–25534
67. S. Pramanik, V. Bhalla and M. Kumar, New J. Chem., 2017, 41, 4806–4813
68. L. M. Mesquita, V. Andre, C. V. Esteves, T. Palmeira, M. N. B. Santos, P. Mateus and R. Delgado, Inorg. Chem., 2016, 55, 2212–2219
69. M. Noboru, K. Yozo and K. Masao, Bull. Chem. Soc. Jpn., 1956, 29, 373–379
70. J. M. Castagnetto and J. W. Canary, Chem. Commun., 1998, 203–204
71. . M. Brouwer, Pure Appl. Chem., 2011, 83, 2213–2228
72. J. R. Lakowicz, Principles of Fluorescence Spectroscopy, 3rd edn, Springer, 2006
73. P. N. Basa and A. G. Sykes, J. Org. Chem., 2012, 77, 8428–8434
74. L. Praveen, C. H. Suresh, M. L. P. Reddy and R. L. Varma, Tetrahedron Lett., 2011, 52, 4730–4733
75. A. D. Becke, J. Chem. Phys., 1993, 98, 5648–5652
76. M. J. Frisch, G. W. Trucks, H. B. Schlegel, G. E. Scuseria, M. A. Robb, J. R. Cheeseman, G. Scalmani, V. Barone, B. Mennucci, G. A. Petersson, H. Nakatsuji, M. Caricato, X. Li, H. P. Hratchian, A. F. Izmaylov, J. Bloino, G. Zheng, J. L. Sonnenberg, M. Hada, M. Ehara, K. Toyota, R. Fukuda, J. Hasegawa, M. Ishida, T. Nakajima, Y. Honda, O. Kitao, H. Nakai, T. Vreven, J. A. Montgomery Jr., J. E. Peralta, F. Ogliaro, M. Bearpark, J. J. Heyd, E. Brothers, K. N. Kudin, V. N. Staroverov, T. Keith, R. Kobayashi, J. Normand, K. Raghavachari, A. Rendell, J. C. Burant, S. S. Iyengar, J. Tomasi, M. Cossi, N. Rega, J. M. Millam, M. Klene, J. E. Knox, J. B. Cross, V. Bakken, C. Adamo, J. Jaramillo, R. Gomperts, R. E. Stratmann, O. Yazyev, A. J. Austin, R. Cammi, C. Pomelli, J. W. Ochterski, R. L. Martin, K. Morokuma, V. G. Zakrzewski, G. A. Voth, P. Salvador, J. J. Dannenberg, S. Dapprich, A. D. Daniels, O. Farkas, J. B. Foresman, J. V. Ortiz, J. Cioslowski and D. J. Fox, Gaussian 09, Revision C.01, Gaussian, Inc., Wallingford, CT, 2010 A. D. Becke, Phys. Rev. A: At., Mol., Opt. Phys., 1988, 38, 3098–3100
77. C. Lee, W. Yang and R. G. Parr, Phys. Rev. B: Condens. Matter Mater. Phys., 1988, 37, 785–789
78. G. Scalmani, M. J. Frisch, B. Mennucci, J. Tomasi, R. Cammi and V. Barone, J. Chem. Phys., 2006, 124, 094107
79. M. Cossi, N. Rega, G. Scalmani and V. Barone, J. Comput. Chem., 2003, 24, 669–681
80. (a) B. Valeur, Molecular Fluorescence: Principles and Applications, Wiley-VCH, Weinheim, 2002 Search PubMed ; (b) P. Thordarson, Chem. Soc. Rev., 2011, 40, 1305–1323
81. (a) SAINT and XPREP, ed. G. M. Sheldrick, Siemens Industrial Automation Inc., Madison, WI, 5.1 edn, 1995 Search PubMed ; (b) SADABS, Empirical Absorption Correction Program, University of Göttingen, Germany, 1997
82. G. M. Sheldrick, SHELXTL Reference Manual, Version 5.1, Bruker AXS, Madison, WI, 1997 Search
83. G. M. Sheldrick, SHELXL-97, Program for Crystal Structure Refinement, University of Göttingen, Germany, 1997
84. A. L. Spek, PLATON-97, University of Utrecht, The Netherlands, 1997
85. Mercury 3.8 (supplied with Cambridge Structural Database); CCDC, Cambridge, U.K, 2004.